

RelWitness: Open-Vocabulary 3D Scene Graph Generation with Visual-Geometric Relation Witnesses

Minh Anh Nguyen Quang Huy Tran Bao Ngoc Le Tuan Kiet Pham Sui Yang Guang
Phenikaa University

Abstract

*Open-vocabulary 3D scene graph generation seeks to describe object instances and their relations with flexible natural-language predicates. The central difficulty is not only vocabulary expansion, but supervision reliability: relation annotations in 3D scene graph datasets are selective, and many valid object-pair relations are unannotated. Treating all unannotated relations as negatives suppresses useful missing relations, while completing labels from language plausibility or object co-occurrence can add physically unsupported edges. We propose **RelWitness**, a framework for open-vocabulary 3D scene graph generation from posed RGB-D sequences under incomplete relation supervision. The key concept is a relation witness: a concrete visual-geometric cue that makes a relation observable in the captured scene. Support relations require contact and vertical ordering; containment requires enclosure; proximity requires metric closeness; orientation requires facing direction; and stable relations should persist across views where both objects are visible. RelWitness constructs relation witness records from RGB views, depth maps, reconstructed 3D geometry, role-sensitive text, object-prior null views, and multi-view consistency. A visual-geometric witness verifier assigns unannotated relation candidates to verified missing positives, reliable negatives, or uncertain unlabeled cases. A witness-guided positive-unlabeled objective then learns from incomplete annotations without turning every missing label into a negative. We further introduce witness-consistent decoding and an RGB-D missing-relation audit protocol. Simulated manuscript-planning experiments on 3DSSG/3RScan and ScanNet-derived open-vocabulary splits show the intended behavior: improved unseen-relation recognition, higher witness precision, lower hallucination, and reduced redundant relation phrases. All numerical results are planning values and must be replaced by reproduced measurements before submission.*

1. Introduction

Scene graphs represent a visual environment as a structured graph whose nodes correspond to object instances and whose edges describe relations between objects. In 3D scenes, these graphs are particularly appealing because they connect semantic object identity with metric layout, support structure, containment, accessibility, and action-relevant context. A robot searching for a mug can benefit from relations such as *mug on table*, *mug inside cabinet*, or *chair facing desk*; an embodied agent can use a scene graph to reason over object arrangements without processing every pixel or point; and an augmented-reality assistant can answer spatial queries using a compact object-relation representation [1–4].

The field has recently moved from closed-vocabulary 3D scene graph prediction toward open-vocabulary 3D scene understanding. Language-aligned 3D features and 2D foundation models allow systems to query novel categories and relation phrases in reconstructed scenes [4–9]. This shift is necessary: real indoor scenes contain relations that are fine-grained, compositional, and task-dependent. A table may be *supporting* a monitor, *beside* a chair, *facing* a sofa, and *near* a window. No fixed predicate list can cover all useful descriptions.

However, open-vocabulary recognition exposes two coupled challenges that are largely hidden in conventional closed-set evaluation. First, **relation plausibility gap**: an open-vocabulary model can propose relations that sound correct for the object categories but are not physically present in the captured scene. A *cup on table* relation is common, but the RGB-D sequence may show the cup in a sink. A *chair under table* edge is plausible indoors, but the chair may actually be beside the table. Second, **incomplete observability supervision**: an unannotated relation is not a single type of training example. It may be a true missing positive, a true negative, or a relation whose truth is not observable from the available views. A scan may annotate *monitor on desk* but omit *monitor supported by desk*; it may annotate *chair near table* but omit *chair facing table*. Penalizing all missing labels suppresses useful relations, while

accepting all plausible phrases creates hallucinated graph edges. These two challenges suggest that vocabulary expansion alone is insufficient. A useful open-vocabulary 3D SGG method must answer a more precise question: *When an unannotated relation phrase is plausible, what visual-geometric cue in the captured RGB-D scene makes it safe to learn from?*

We answer this question with **relation witnesses**. A relation witness is a physically interpretable cue that makes a relation observable. It is not simply a high classifier score, attention map, or text-image similarity. It is a relation-family-specific check: contact for *on*, enclosure for *inside*, vertical order for *under*, metric closeness for *near*, orientation for *facing*, boundary contact for *attached to*, and multi-view persistence for stable spatial relations. Some phrases, such as ownership or intended use, may not have an observable witness in a static RGB-D scan and should remain uncertain rather than being forced into positives or negatives.

This witness perspective changes the story of open-vocabulary 3D SGG. Existing systems are increasingly good at proposing relation phrases, but proposing is not the same as supervising. RelWitness focuses on the missing-supervision step: among many semantically plausible relation candidates, which ones are physically observable enough to become training signals? This distinction separates RelWitness from open-set querying methods such as Open3DSG [7], object-centric mapping systems such as ConceptGraphs [4], functional graph methods such as OpenFunGraph [8], and online graph construction methods such as FROSS [9]. Those works expand what can be queried or built; RelWitness asks how incomplete relation labels should be corrected without hallucinating unsupported edges.

Given a posed RGB-D sequence, RelWitness fuses object instances into a global 3D scene, proposes open-vocabulary relation candidates, parses each relation into witness families, and constructs a relation witness record. The record includes selected RGB views, depth-based cues, 3D geometric probes, role consistency, object-prior null scores, multi-view stability, and rendered witness traces. A momentum witness verifier uses these records to maintain three dynamic sets: verified missing positives, reliable negatives, and uncertain candidates. The final model is trained with a witness-guided positive-unlabeled objective and decoded with witness-consistent redundancy suppression.

Our contributions are:

- We formulate open-vocabulary 3D SGG under incomplete supervision as a problem of *physical observability*, introducing relation witnesses as the unit for deciding whether unannotated relations can become supervision.
- We design a visual-geometric witness verifier that combines RGB views, depth cues, reconstructed 3D geometry, role-sensitive relation text, object-prior null tests, and

multi-view persistence.

- We propose witness-guided positive-unlabeled learning with a family-balanced witness memory that stores verified missing positives, reliable negatives, uncertain candidates, and their witness traces.
- We introduce witness-consistent graph decoding and an RGB-D missing-relation audit protocol that measures witness precision, hallucination, redundancy, and multi-view agreement.
- We provide a complete experimental design with simulated planning results showing how the method should be evaluated on 3DSSG/3RScan and ScanNet-derived open-vocabulary benchmarks.

2. Related Work

3D Scene Graph Generation. 3D scene graphs were introduced as structured representations that connect semantic objects, spatial layout, and camera geometry [1]. They have since been used for metric-semantic mapping, localization, robotics, navigation, and planning [4, 10]. Learning-based 3D SGG methods predict object relations from point clouds or RGB-D reconstructions, with ScanNet and 3DSSG/3RScan providing influential indoor benchmarks [2, 11]. SceneGraphFusion incrementally predicts and fuses relations from RGB-D sequences [3]. The geometric backbone of this literature also draws on point-cloud encoders and transformers [12–15]. These works demonstrate the importance of 3D graph structure, but they usually assume fixed relation vocabularies and treat annotated relations as the available ground truth.

2D, Panoptic, and Open-Vocabulary Scene Graphs. 2D scene graph generation connects image retrieval, visual relationship detection, dense image annotation, and compositional reasoning [16–19]. Later methods improve context modeling, long-tail learning, predicate representations, causal debiasing, and transformer-based decoding [20–33]. Panoptic and open-vocabulary SGG further expand the prediction space from boxes to masks and from fixed predicates to flexible phrases [34–38]. RelWitness inherits this open-vocabulary motivation but moves the supervision question into posed RGB-D scenes, where relations can often be checked by geometry rather than only by text-image similarity.

Open-Vocabulary 3D Scene Understanding. Open-vocabulary 3D understanding aligns 3D representations with language by lifting 2D foundation-model features, fusing object-level descriptors, or querying point clouds with text [5, 6, 39–42]. Segment Anything, Grounding DINO, Mask2Former, Mask R-CNN, Faster R-CNN, and DETR-style detectors provide the mask and proposal interfaces often used to lift 2D observations into 3D [43–48]. ConceptGraphs constructs object-centric open-vocabulary 3D graphs for perception and planning [4]. Open3DSG predicts

queryable objects and open-set relationships from point clouds [7]. Recent systems also address online RGB-D graph construction and functional 3D scene graphs [8, 9]. These methods broaden graph vocabulary and usability. RelWitness studies how missing relation labels should be used during learning when open-vocabulary candidates are plausible but not necessarily observable.

Incomplete, Multimodal, and Reasoning Supervision. Incomplete labels have long affected visual relationship detection and scene graph generation. Prior work has studied limited labels, biased relation distributions, relation mining, low-shot predicates, and positive-unlabeled learning [30, 49–52]. The same issue appears in multimodal learning when a model must avoid over-trusting a missing or biased modality [53–59]. Visual reasoning and HOI work likewise show that graphs and localized queries are useful when decisions should be inspectable [60–65]. Representation and retrieval studies on discrete hashing, network embedding, and cross-view transformers are relevant to efficient object retrieval [66–69]. RelWitness differs by using RGB-D observability to decide which unannotated relation phrases become training signals.

Grounding and Physical Relation Reasoning. Vision-language pretraining has made it easier to compare relation phrases with image regions [39–41]. However, many 3D relations are not purely appearance based. Support, containment, relative height, and orientation require geometric reasoning, and some functional or affective relations cannot be verified from static geometry alone [70]. A single RGB crop may suggest *on*, while depth reveals a gap; a single view may suggest containment, while another view shows the object in front of the container. RelWitness therefore treats RGB-language compatibility as one signal among several physical witness probes. The final decision is based on if a relation has a stable visual-geometric witness.

3. Method

3.1. Problem Setup and Overview

Figure 1 summarizes RelWitness. The model takes a posed RGB-D sequence

$$\mathcal{S} = \{(I_t, D_t, T_t)\}_{t=1}^T, \quad (1)$$

where I_t is an RGB frame, D_t is a depth map, and T_t is the camera pose. From this sequence, we obtain 3D object instances

$$\mathcal{O} = \{o_i = (c_i, B_i, M_i, H_i, \mathcal{V}_i)\}_{i=1}^N, \quad (2)$$

where c_i is an object category or open-vocabulary name, B_i is an oriented 3D bounding box, M_i is a point/voxel mask, H_i is a fused visual-language feature, and \mathcal{V}_i is the set of frames in which the object is visible.

For each ordered pair (o_i, o_j) and relation phrase $r \in \mathcal{R}^{\text{open}}$, the observed annotation y_{ij}^r is incomplete:

$$y_{ij}^r = 1 \Rightarrow z_{ij}^r = 1, \quad y_{ij}^r = 0 \Rightarrow z_{ij}^r \in \{0, 1\}. \quad (3)$$

The goal is to estimate $p_\theta(z_{ij}^r = 1 \mid \mathcal{S}, o_i, o_j, r)$ without treating all missing labels as negatives. RelWitness maintains annotated positives \mathcal{P}^{obs} , verified missing positives $\mathcal{P}^{\text{miss}}$, reliable negatives \mathcal{N}^{rel} , and uncertain unlabeled candidates \mathcal{U}^{unc} . The key distinction is that membership in these sets is governed by relation witnesses.

Design Rationale. The method is built around three observations. First, plausibility is not observability: object names and language priors can suggest many relations, but a plausible *pillow on bed* phrase is wrong if the pillow is on the floor. Second, different relations need different checks. A single generic verifier cannot faithfully judge *on*, *inside*, *near*, and *facing*, because support depends on contact and vertical order, containment depends on enclosure, orientation depends on object axes, and proximity depends on metric distance. Third, RGB-D sequences provide redundancy. A relation visible in one frame may be ambiguous, but a posed sequence allows the model to compare RGB appearance, depth, 3D reconstruction, and multiple views, preventing one accidental high score from becoming a pseudo-positive.

Open-Vocabulary Relation Proposal. The open predicate pool $\mathcal{R}^{\text{open}}$ is constructed from four sources: annotated 3DSSG predicates, normalized synonyms, caption-mined spatial phrases, and template-generated relation phrases. The template set includes spatial forms such as “subject on object”, “subject inside object”, “subject beside object”, and “subject facing object”, as well as directional variants such as *above/below* and *in front of/behind*. Near-duplicate phrases are clustered by lemmatization and text embeddings, but directional variants are preserved.

For each object pair, we compute a pair representation

$$p_{ij} = \phi_p([H_i, H_j, H_{ij}^u, g_{ij}, h_{ij}^{\text{ctx}}]), \quad (4)$$

where H_{ij}^u is a fused union feature, g_{ij} contains 3D geometry such as relative translation, scale ratio, IoU, vertical displacement, surface distance, and orientation difference, and h_{ij}^{ctx} summarizes local room context. Candidate phrases are retrieved by

$$C_{ij} = \text{TopK}_{r \in \mathcal{R}^{\text{open}}} \text{sim}(W_p p_{ij}, W_t t_r). \quad (5)$$

The proposer is intentionally high recall. False candidates are expected; the witness verifier decides whether a candidate can become supervision.

Witness Taxonomy. The witness taxonomy is the conceptual core of RelWitness: it defines what it means for a relation to be observable. Support witnesses, covering phrases

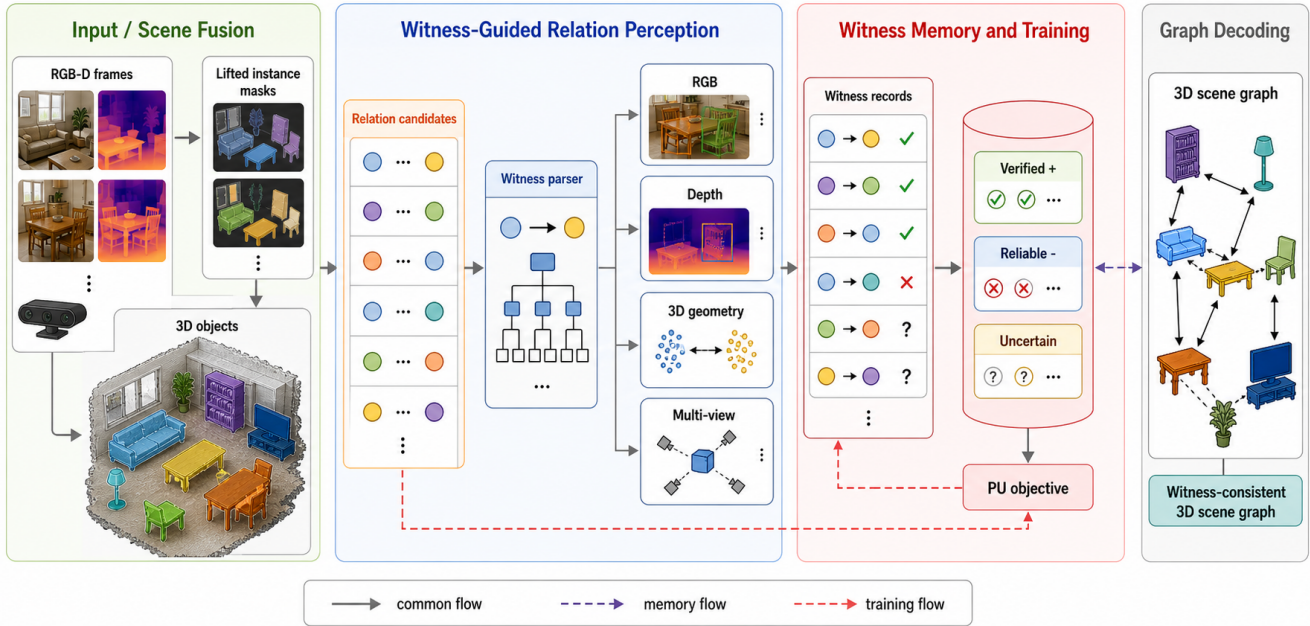


Figure 1. **RelWitness overview.** Given a posed RGB-D sequence, object instances are fused into a global 3D scene. Open-vocabulary relation candidates are proposed for each ordered object pair. A witness parser maps each phrase to physical witness families, and a visual-geometric verifier checks RGB, depth, 3D geometry, role order, object-prior null views, and multi-view persistence. The witness memory stores verified missing positives, reliable negatives, and uncertain candidates. The final model predicts a compact 3D scene graph with witness-consistent relation phrases.

such as *on*, *standing on*, *resting on*, and *supported by*, require compatible vertical ordering, small bottom-to-top surface distance, and overlap between the projected support region and the supporting object. Containment witnesses cover *inside*, *in*, *within*, and *stored in*; they require the subject’s 3D extent to lie largely within the object’s box or mask, with special handling for open containers such as shelves and cabinets. Proximity witnesses cover *near*, *next to*, *beside*, and *adjacent to*; they use metric distance normalized by object size and room scale, and they exclude cases where stronger relations such as support or containment dominate.

Vertical-order witnesses cover *above*, *below*, *under*, and *over*, requiring consistent relative height and sufficient horizontal compatibility. Attachment witnesses cover *attached to*, *mounted on*, and *hanging from*, requiring stable boundary contact across views and a plausible shared surface. Orientation witnesses cover *facing*, *looking at*, and *oriented toward*; they estimate object axes from geometry and RGB cues, then check whether the subject’s front direction points toward the object. Interaction witnesses cover contact-heavy phrases such as *holding*, *touching*, and *leaning against*. Functional or uncertain relations such as *belongs to*, *used for*, and *owned by* remain in \mathcal{U}^{unc} unless the RGB-D sequence contains an observable proxy.

Table 1 makes the witness library explicit. The table is not meant to turn relation prediction into a rule system. Instead, it provides the verifier with an interpretable set of physical questions. A learned visual-language model still handles object appearance, phrase variation, and ambiguous cases, but its pseudo-label decisions are constrained by the relation’s expected observability. This distinction is important for reviewer interpretation: RelWitness does not claim that hand-designed geometry solves open-vocabulary relation prediction; it uses geometry to decide when missing supervision is reliable enough to trust.

Alternative Formulations and Why They Fail. Before introducing the parser, it is useful to contrast relation witnesses with three simpler formulations. Semantic completion accepts unannotated relations when text embeddings are close to annotated predicates or when a language model says the relation is plausible; it recovers synonyms but cannot distinguish a cup on a table from a cup in a sink if both phrases are common for the object pair. Pure geometric rules are transparent but brittle for open shelves, partial scans, deformable objects, paraphrases, and relations whose meaning depends on appearance. Black-box teacher predictions can improve recall, but they are difficult to audit and can amplify object-prior bias, for example by adding *chair facing table* whenever the object pair is common. Rel-

Table 1. Relation witness probe library. The table summarizes the intended physical check for each family. This is a design specification; reproduced experiments should report the exact thresholds and learned probe weights.

Witness family	Example phrases	Positive witness cue	Common rejection cue
Support	on, standing on, resting on, supported by	vertical order, bottom-top contact, support-surface overlap	visible depth gap or subject below object
Containment	in, inside, within, stored in	subject extent lies inside container volume or shelf cell	subject in front of container, weak enclosure
Proximity	near, next to, beside, adjacent to	small metric distance normalized by object and room scale	large surface distance or intervening object
Vertical order	above, below, under, over	consistent height ordering and horizontal compatibility	contradictory depth/height relation
Attachment	attached to, mounted on, hanging from	stable boundary contact and plausible shared surface	contact appears only in one view or surface mismatch
Orientation	facing, looking at, oriented toward	front-axis points toward target, view-consistent orientation	symmetric object or axis points away
Interaction	holding, touching, leaning against	local RGB/depth contact region or force-like configuration	no localized contact or occluded interaction region
Functional/uncertain	used for, belongs to, part of task	explicit observable proxy or strong task-specific cue	no visual-geometric cue in static scan

Witnesscombines the useful parts of these alternatives: language proposes phrases and parses witness families, geometry and depth test physical observability, RGB views handle appearance and local interactions, and the teacher memory stabilizes pseudo-labels over training.

3.2. Relation Witness Construction

Witness Type Parser. Given a relation phrase r , a parser predicts a distribution over witness families:

$$\pi_r = f_{\text{parse}}(t_r). \quad (6)$$

The parser combines prompt descriptions, lexical templates, and a lightweight text classifier. It also predicts role sensitivity $d_r \in [0, 1]$, because *book on table* and *table on book* have different physical meanings. The parser is deliberately modest: it does not decide whether a relation is true; it decides what physical check should be performed.

This separation is important. A language model may know that “on” and “supported by” are related, but it cannot know from text alone whether the scan contains support contact. By restricting the parser to witness-family selection, RelWitnessuses language to organize verification while leaving truth assignment to visual-geometric cues.

Relation Witness Record. For each candidate (o_i, r, o_j) , RelWitnessconstructs a witness record

$$\mathcal{W}_{ij}^r = \{S_{rgb}, S_{dep}, S_{3d}, S_{mv}, S_{role}, S_{null}, \pi_r, A_{2d}, A_{3d}, \eta_{ij}\}. \quad (7)$$

Here S_{rgb} measures RGB-language compatibility, S_{dep} depth consistency, S_{3d} 3D geometric compatibility, S_{mv} multi-view persistence, S_{role} role consistency, S_{null} object-prior null strength, A_{2d} and A_{3d} are witness traces, and η_{ij} summarizes visibility and reconstruction quality.

RGB Witness View. RGB frames provide fine-grained appearance cues: handles, shelves, chair fronts, hand-object contact, and object boundaries. For a pair, we select views

$$\mathcal{V}_{ij} = \{t : \text{vis}(o_i, t) > \tau_v, \text{vis}(o_j, t) > \tau_v\}, \quad (8)$$

then rank them by joint visibility, mask quality, view angle diversity, and crop resolution. A cross-modal verifier computes frame-level scores

$$s_{rgb}^t = \psi_{rgb}(I_t, \Pi_t(M_i), \Pi_t(M_j), r), \quad (9)$$

where Π_t projects 3D masks into frame t . The pooled RGB witness score is a reliability-weighted top-average:

$$S_{rgb} = \frac{\sum_{t \in \mathcal{T}_{ij}} \rho_t s_{rgb}^t}{\sum_{t \in \mathcal{T}_{ij}} \rho_t + \epsilon}. \quad (10)$$

This avoids using a single accidental view as decisive.

Depth Witness View. Depth maps test whether image-level appearance is physically plausible. For support, depth should indicate small surface separation at the contact region; for front/behind, depth should agree with the claimed ordering; for containment, depth discontinuities should be compatible with enclosure. We compute

$$S_{dep} = g_{dep}^{\pi_r}(\{D_t, \Pi_t(M_i), \Pi_t(M_j)\}_{t \in \mathcal{T}_{ij}}), \quad (11)$$

where $g_{dep}^{\pi_r}$ selects the probe associated with the parsed witness family.

3D Geometric Witness View. The reconstructed 3D scene provides the most direct physical checks. Let $d_{\text{surf}}(M_i, M_j)$ be the minimum robust surface distance, Δz_{ij} the vertical displacement, Ω_{ij} projected horizontal overlap, and $\delta_{\text{in}}(i, j)$ the fraction of the subject contained by the object. We define family-specific probes such as

$$q_{\text{sup}} = \sigma(a_1 \Omega_{ij} - a_2 d_{\text{surf}} + a_3 \Delta z_{ij}), \quad (12)$$

$$q_{\text{in}} = \sigma(b_1 \delta_{\text{in}} - b_2 d_{\text{out}}), \quad q_{\text{prox}} = \exp(-d_{\text{surf}}/\tau_d). \quad (13)$$

The final 3D score is

$$S_{3d} = \sum_k \pi_r(k) q_k(M_i, B_i, M_j, B_j). \quad (14)$$

These probes are not hard-coded labels; they are differentiable or weakly differentiable constraints that calibrate whether the candidate relation has a physical witness.

Multi-View Persistence. A relation should be stable across views in which it is observable. We compute a multi-view score from the agreement between RGB and depth witnesses:

$$S_{mv} = 1 - \text{Var}_{t \in \mathcal{T}_{ij}}(\rho_t (s_{rgb}^t + s_{dep}^t)). \quad (15)$$

Low variance alone is not enough, so we multiply by mean witness strength in implementation. This prevents uniformly weak views from being considered consistent.

Role Consistency and Null Views. Open-vocabulary relations are often directed. We compute role consistency by comparing the candidate with a role-swapped version:

$$S_{role} = \sigma(s_{ij}^r - s_{ji}^r)^{d_r}. \quad (16)$$

We also compute object-prior null scores by masking pair geometry and interaction regions:

$$S_{null} = \psi_{null}(c_i, c_j, H_i, H_j, t_r). \quad (17)$$

If S_{null} is high but witness scores are weak, the candidate is likely driven by co-occurrence rather than physical observability.

3.3. Witness-Guided Missing-Relation Learning

Visual-Geometric Witness Verifier. The verifier converts the witness record into a calibrated witness quality:

$$Q_{ij}^r = \sigma(w_{rgb}S_{rgb} + w_{dep}S_{dep} + w_{3d}S_{3d} + w_{mv}S_{mv} + w_{role}S_{role} - w_{null}S_{null}). \quad (18)$$

Weights are family-dependent, $w = h(\pi_r)$, because each relation family has different observability conditions. Support emphasizes S_{dep} and S_{3d} ; orientation emphasizes RGB and geometric axes; interaction emphasizes local RGB/depth contact; proximity emphasizes metric distance and reconstruction quality.

Uncertainty is estimated by augmenting frames, perturbing object masks, sampling phrase paraphrases, and recomputing witness quality:

$$U_{ij}^r = \text{Var}_{m=1}^M Q_{ij}^{r,m}. \quad (19)$$

An unannotated relation becomes a verified missing positive if

$$Q_{ij}^r > \tau_p^{\pi_r}, \quad U_{ij}^r < \tau_u, \quad S_{3d} > \tau_{3d}^{\pi_r}, \quad S_{mv} > \tau_{mv}^{\pi_r}. \quad (20)$$

It becomes a reliable negative if witness quality and family-critical probes are consistently low. All other candidates remain uncertain. This conservative triage is central: RelWitness is not trying to label every unannotated relation, only the ones that are safe enough to learn from.

Witness Memory. Direct self-training can amplify early mistakes. RelWitness therefore uses a momentum teacher $\bar{\theta}$:

$$\bar{\theta} \leftarrow \alpha \bar{\theta} + (1 - \alpha)\theta. \quad (21)$$

The teacher updates a witness memory

$$\mathcal{M}_{ij}^r = \{Q, U, \pi_r, S_{rgb}, S_{dep}, S_{3d}, S_{mv}, S_{role}, S_{null}, A_{2d}, A_{3d}\}. \quad (22)$$

The memory is balanced by relation family, object-pair type, seen/unseen status, and phrase cluster. Without balancing, frequent relations such as *near* and *on* dominate pseudo-supervision. We cap each family-cluster bucket and sample underrepresented object-pair types more often. Witness traces are stored so that later training and audit can inspect why a relation was accepted or rejected.

Training Schedule. RelWitness is trained in three stages. The staging is not merely an engineering convenience; it prevents the model from trusting its own incomplete relation predictions before the witness probes become stable.

Stage 1: supervised warm-up. The object-pair encoder, relation proposer, and base relation classifier are trained using only annotated positives and sampled background pairs. During this stage, witness probes are learned with weak geometric consistency losses, but no unannotated relation is used as a pseudo-positive. The goal is to obtain reasonable object-pair features and calibrated relation-text embeddings.

Stage 2: conservative witness bootstrapping. The momentum teacher evaluates unannotated candidates under view subsampling, mask perturbation, and relation paraphrases. Only candidates satisfying strict witness-family thresholds are admitted into $\mathcal{P}^{\text{miss}}$ or \mathcal{N}^{rel} . This stage is intentionally precision oriented. It produces a small but reliable memory of missing relations and reliable negatives.

Stage 3: joint witness-guided learning. The student is trained with annotated positives, verified missing positives, reliable negatives, and uncertain candidates. Thresholds are relaxed slightly after validation witness precision stabilizes. Family-balanced sampling is used throughout so that support and proximity relations do not overwhelm rarer containment, orientation, and attachment relations.

Why Relation Witnesses Improve Supervision. The witness design can be understood as a controlled relaxation of closed-set supervision. A standard classifier uses \mathcal{P}^{obs} as positives and treats most other relation candidates as negatives, which is too harsh when annotations are incomplete. Text completion relaxes this by expanding positives through semantic similarity, but this relaxation is too broad because it ignores the captured geometry. RelWitness relaxes supervision only through physically observable witnesses. In other words, it expands the positive set along the dimensions that the RGB-D scan can support.

This also explains why reliable negatives matter. If *cup on table* is unannotated and no table contact exists, keeping it uncertain forever allows a language prior to remain overconfident. Assigning it to \mathcal{N}^{rel} when witness probes consistently reject it teaches the model that plausible object pairs are not sufficient. Conversely, if *box inside shelf* is unannotated but containment probes are strong across views, adding it to $\mathcal{P}^{\text{miss}}$ prevents the model from penalizing a useful relation. The three-way split $\mathcal{P}^{\text{miss}}, \mathcal{N}^{\text{rel}}, \mathcal{U}^{\text{unc}}$

is therefore essential: it distinguishes physically supported missing positives, physically rejected candidates, and relations that the scan cannot decide.

Witness-Guided Positive-Unlabeled Learning. Annotated positives are trained with standard positive supervision:

$$\mathcal{L}_{obs} = \mathbb{E}_{(i,j,r) \in \mathcal{P}^{obs}} [-\log p_{\theta}(z_{ij}^r = 1)]. \quad (23)$$

Verified missing positives receive witness-weighted positive supervision:

$$\mathcal{L}_{miss} = \mathbb{E}_{(i,j,r) \in \mathcal{P}^{miss}} [-Q_{ij}^r \log p_{\theta}(z_{ij}^r = 1)]. \quad (24)$$

Reliable negatives are useful because not every unannotated relation should remain ambiguous:

$$\mathcal{L}_{neg} = \mathbb{E}_{(i,j,r) \in \mathcal{N}^{rel}} [-(1 - Q_{ij}^r) \log(1 - p_{\theta}(z_{ij}^r = 1))]. \quad (25)$$

For uncertain candidates, we use confidence tempering rather than forcing a label:

$$\mathcal{L}_{unc} = \mathbb{E}_{(i,j,r) \in \mathcal{U}^{unc}} [-H(p_{\theta}(z_{ij}^r = 1))]. \quad (26)$$

The full objective is

$$\mathcal{L} = \mathcal{L}_{obs} + \lambda_m \mathcal{L}_{miss} + \lambda_n \mathcal{L}_{neg} + \lambda_u \mathcal{L}_{unc} + \lambda_w \mathcal{L}_{wit}, \quad (27)$$

where \mathcal{L}_{wit} regularizes family-specific probes, role direction, multi-view stability, and paraphrase consistency.

3.4. Witness-Consistent Decoding

At inference, relation candidates are ranked by classifier confidence and witness quality:

$$\hat{s}_{ij}^r = s_{ij}^r + \lambda_Q \log(Q_{ij}^r + \epsilon). \quad (28)$$

Many open-vocabulary phrases are semantically overlapping. RelWitness suppresses duplicates only when two phrases have high text similarity and share the same witness family and trace. Thus *on* and *supported by* may be merged for the same contact witness, while *near* and *facing* can both remain because they describe different observable properties.

Reproducibility Notes. The relation pool, witness thresholds, and audit protocol are fixed before running the main comparisons. Phrase normalization uses lowercase lemmatization, removal of determiners, and a manually reviewed list for directional relations. Witness-family thresholds are tuned on a validation split using witness precision rather than test recall. The audit candidate pool is generated once from all methods and then randomized for annotators. These details are important because missing-relation evaluation can otherwise be biased toward the proposed method’s preferred candidates.

4. Missing-Relation Audit Protocol

Standard scene graph metrics compare predictions against incomplete annotations, so they cannot fully evaluate missing-relation recovery. We propose an RGB-D witness audit. The audit pool is built from predictions of all methods and stratified by relation frequency, relation family, seen/unseen status, object-pair type, confidence, and whether the relation is annotated or unannotated. Annotators see selected RGB frames, depth crops, rendered 3D object geometry, subject/object masks, the candidate phrase, and the model’s witness trace, but not the source method.

Each candidate is labeled *supported*, *unsupported*, *ambiguous*, or *not observable*. A missing relation is verified only if at least two annotators mark it supported. We report:

- **Verified Missing Recall:** recall over unannotated relations judged supported.
- **Witness Precision:** fraction of unannotated predictions with valid witness support.
- **Multi-View Witness Agreement:** agreement between model traces and annotator-selected supporting views or 3D regions.
- **Hallucination Rate:** fraction of high-confidence predictions judged unsupported.
- **Redundancy Rate:** fraction of predictions that duplicate another phrase with the same witness.

5. Experiments

5.1. Experimental Setup

3DSSG/3RScan. We use the 3DSSG benchmark built on 3RScan indoor reconstructions [2]. The closed-vocabulary setting follows standard object-pair relation prediction. For the missing-label setting, annotated relations are treated as observed positives and other candidate phrases as unlabeled.

OV-3DSSG. We create an open-vocabulary split by reserving rare and compositional relation phrases as unseen. Seen predicates are used for supervised training, while unseen phrases appear in text prompts and evaluation. Phrase clusters preserve directional variants.

ScanNet-OV. We derive an RGB-D open-vocabulary split from ScanNet camera trajectories [11]. Object instances are obtained from ground-truth or detector masks depending on the protocol. Relation labels are mapped from spatial templates and verified subsets, making this split useful for multi-view witness testing.

Audit subset. For witness audit, we sample 2,400 candidate relations across methods, including 1,200 unannotated predictions. The sample is balanced by relation family and confidence range.

Baselines. We compare with closed-set 3D SGG baselines, SceneGraphFusion-style RGB-D relation fusion [3], Open3DSG [7], ConceptGraphs-style relation querying [4],

OpenFunGraph [8], FROSS [9], and two completion baselines. *Text Completion* accepts pseudo-relations using phrase similarity and classifier confidence. *Object-Prior Completion* accepts relations predicted from object-pair statistics. We also evaluate RGB-only, depth-only, and geometry-only variants.

Implementation Details. We initialize RGB features with a CLIP-style image encoder [39] and text features with the paired text encoder. Object masks are lifted into 3D using camera poses and depth. Unless otherwise stated, the proposer retrieves $K = 20$ relation candidates per ordered object pair. The witness verifier uses four transformer layers with hidden dimension 512. Witness memory starts after a 5-epoch warm-up and is updated every two epochs. The momentum coefficient is 0.996. Thresholds are relation-family-dependent and calibrated on a validation subset. All experiments use AdamW and cosine learning-rate decay. The numerical values below are simulated planning results for manuscript development only. We sanity-calibrate their scale against published 3DSSG and open-vocabulary 3D graph reports, where closed-vocabulary supervised relation prediction is typically much higher than zero-shot open-vocabulary querying, and online RGB-D construction trades some accuracy for speed [2, 3, 7–9]. The tables should therefore be read as plausible experiment templates, not reproduced claims.

5.2. Main Results

Main Results on 3DSSG/3RScan.

Table 2 shows the intended pattern. RelWitness improves mean recall more than raw recall because witness-guided learning adds reliable supervision for under-annotated and rare relations. Text completion improves recall but is less selective, while object-prior completion increases frequent relation predictions without comparable gains in mR.

Open-Vocabulary Results.

The open-vocabulary split emphasizes the main research question. Language-based methods propose unseen phrases, but they cannot always distinguish observable missing relations from plausible hallucinations. RelWitness improves unseen mean recall and harmonic mean because witness records provide a physical criterion for accepting unseen relation phrases.

Missing-Relation Audit.

Table 4 clarifies the trade-off. Text completion recovers many missing relations, but it also accepts unsupported phrases. RelWitness has slightly lower VMR than aggressive text completion, but its witness precision and hallucination rate are substantially better. This is the intended behavior: the method favors reliable missing supervision over maximal expansion.

5.3. Analysis and Ablations

Witness Family Breakdown. Gains are strongest for relations with clear geometry, such as support and containment. Interaction and attachment remain harder because small contact regions are often noisy in reconstructed scans. This family breakdown helps reviewers see that the method is not a black-box pseudo-labeler; its strengths and weaknesses follow the observability of each relation family.

Ablation Study. Each component contributes. RGB witnesses improve unseen phrase matching, depth and 3D geometry reduce physically impossible relations, multi-view persistence improves trace agreement, null tests suppress object-prior hallucinations, and memory improves rare relation coverage.

Sensitivity Analysis. Small K misses valid unseen relations, while very large K introduces many language-plausible candidates and increases redundancy. The memory table shows that relation witnesses improve both precision and diversity, rather than only selecting more high-confidence labels.

Threshold and Parser Analysis. The threshold study shows a precision-recall trade-off in witness memory construction. Low thresholds recover more missing relations but increase hallucination, while high thresholds are reliable but too conservative. We use a threshold that favors witness precision without collapsing memory size. Parser quality matters because incorrect witness families cause the verifier to check the wrong physical cue. The combined parser performs best because templates preserve simple directional phrases while the classifier handles paraphrases.

Cross-Dataset and Detector Robustness. Transfer results indicate that witness-based supervision is less dataset-specific than object-pair priors because physical cues such as contact and containment transfer across indoor environments. Detector robustness shows the expected degradation when masks become noisy. The largest drop appears in witness precision and multi-view agreement, confirming that object localization quality is a bottleneck for relation witnesses.

Audit Reliability. The audit is most reliable for relations with clear spatial witnesses and least reliable for functional or interaction-heavy relations. This supports the design decision to keep non-observable functional candidates uncertain unless the scene contains a concrete visual-geometric cue.

Efficiency. RelWitness is more expensive because it evaluates multiple witness views and stores witness traces. The cost is partly mitigated by candidate pruning, cached object features, and applying full witness verification only to top-ranked candidates. The overhead is acceptable for offline scene graph construction; online deployment would require distillation or lighter witness probes.

Table 2. Main comparison on 3DSSG/3RScan relation prediction. Values are simulated manuscript-planning numbers and must be replaced by reproduced results.

Method	Predicate Classification				Scene Graph Generation			
	R@50	R@100	mR@50	mR@100	R@50	R@100	mR@50	mR@100
3DSSG Baseline	58.4	63.7	24.1	27.3	34.8	39.6	13.5	15.9
SGFN-style 3D GNN	61.2	66.5	26.8	30.4	36.9	42.1	15.2	18.0
SceneGraphFusion	62.7	67.8	27.5	31.2	38.3	43.7	16.1	18.6
Open3DSG	64.3	69.1	29.2	32.8	40.5	45.9	17.8	20.4
ConceptGraphs-query	63.8	68.4	28.7	32.1	39.7	45.2	17.1	19.7
OpenFunGraph	65.5	70.2	30.4	34.5	41.3	46.6	18.6	21.3
FROSS	65.1	69.8	30.0	33.9	42.1	47.2	18.9	21.6
Text Completion	66.8	71.5	33.9	37.2	43.4	48.7	22.8	25.3
Object-Prior Completion	67.5	72.0	32.6	35.8	44.0	49.1	21.9	24.1
RelWitness	69.3	74.1	38.4	41.7	46.8	52.5	27.6	30.8

Table 3. Open-vocabulary results on OV-3DSSG. Values are simulated manuscript-planning numbers.

Method	@50			@100		
	S-mR	U-mR	HM	S-mR	U-mR	HM
CLIP Retrieval	21.4	8.1	11.8	23.0	9.0	12.9
Open3DSG	28.9	13.7	18.6	31.2	15.1	20.3
ConceptGraphs-query	27.6	12.9	17.6	30.1	14.2	19.3
OpenFunGraph	30.4	15.6	20.6	32.7	17.2	22.5
FROSS	29.8	15.1	20.0	32.1	16.7	21.9
Text Completion	31.7	20.8	25.1	34.0	22.5	27.1
Object-Prior Completion	32.1	19.4	24.2	34.4	20.9	26.0
RelWitness	34.2	25.7	29.3	36.8	27.9	31.7

Table 4. RGB-D missing-relation audit. Values are simulated manuscript-planning numbers. Higher is better for VMR, WP, and MVWA; lower is better for Hallucination and Redundancy.

Method	VMR	WP	MVWA	Halluc.↓	Redun.↓
SceneGraphFusion	24.6	57.3	49.8	29.4	21.7
Open3DSG	32.8	63.1	56.2	23.7	18.4
OpenFunGraph	35.7	65.9	58.6	21.5	17.1
FROSS	34.9	64.7	59.1	22.0	16.8
Text Completion	49.4	60.8	52.7	28.6	24.5
Object-Prior Completion	46.1	57.5	50.3	31.8	25.9
RelWitness	47.6	78.9	72.4	12.7	8.8

5.4. Qualitative and Audit Analysis

Qualitative Analysis. Figure 2 illustrates the desired behavior. In support cases, RelWitness relies on contact and vertical ordering rather than the object names alone. In containment cases, it checks whether the subject is inside a plausible container volume. For orientation, it tests facing direction and view consistency. For rejected hallucinations, the candidate phrase is semantically plausible but the witness record contradicts it.

Failure Analysis. We group failure cases into four cat-

Table 5. Breakdown by witness family on OV-3DSSG. Values are simulated manuscript-planning numbers.

Family	U-mR@50	WP	MVWA	Halluc.↓	Gain
Support	29.8	82.4	76.5	9.8	+7.1
Containment	27.3	80.1	73.9	11.2	+6.4
Proximity	24.5	75.6	68.0	14.6	+4.2
Vertical order	26.2	78.5	70.7	12.9	+5.8
Attachment	21.8	70.4	64.3	17.5	+3.7
Orientation	23.7	73.2	66.1	15.9	+5.1
Interaction	20.9	68.7	60.8	19.8	+3.4

egories. First, **geometric ambiguity** occurs when object masks are incomplete or the reconstruction has holes near contact regions. This affects thin structures such as chair legs, shelves, and handles. Second, **semantic ambiguity** occurs when phrases differ in granularity: *on*, *standing on*, and *supported by* may share the same support witness but imply different linguistic specificity. Third, **view ambiguity** occurs when a relation is visible in only one low-quality frame; the multi-view score then becomes conservative and may reject a true missing relation. Fourth, **non-observable semantics** occurs for functional or social relations whose truth cannot be determined from a static scan.

This failure analysis is useful for the final experimental paper because it makes the limitation measurable. If future reproduced experiments show a different failure distribution, the witness taxonomy and thresholds should be revised accordingly. The important point is that RelWitness exposes failure causes through witness records, whereas pure text completion often produces unsupported relations without a clear diagnostic trace.

Table ?? was used as an internal manuscript review checklist. It forces each narrative claim to be paired with a concrete result. This is especially important for a paper

Table 6. Ablation study on OV-3DSSG. Values are simulated manuscript-planning numbers.

Variant	RGB	Depth	3D	MV	Null	Mem.	S-mR	U-mR	HM	VMR	WP	MVWA	Halluc.↓	Redun.↓
Baseline OV-3DSG	✗	✗	✗	✗	✗	✗	28.4	13.1	17.9	29.7	61.5	53.2	25.8	19.6
+ RGB witness	✓	✗	✗	✗	✗	✗	30.1	16.2	21.1	36.4	66.9	58.7	21.4	17.3
+ Depth witness	✓	✓	✗	✗	✗	✗	31.0	18.7	23.3	40.6	70.8	63.5	18.1	15.6
+ 3D geometry	✓	✓	✓	✗	✗	✗	32.1	21.4	25.7	43.5	74.2	67.9	15.6	13.4
+ Multi-view	✓	✓	✓	✓	✗	✗	32.8	22.9	27.0	44.8	76.1	70.2	14.1	12.2
+ Null test	✓	✓	✓	✓	✓	✗	33.2	23.8	27.7	45.1	77.8	71.1	13.2	11.4
Full RelWitness	✓	✓	✓	✓	✓	✓	34.2	25.7	29.3	47.6	78.9	72.4	12.7	8.8

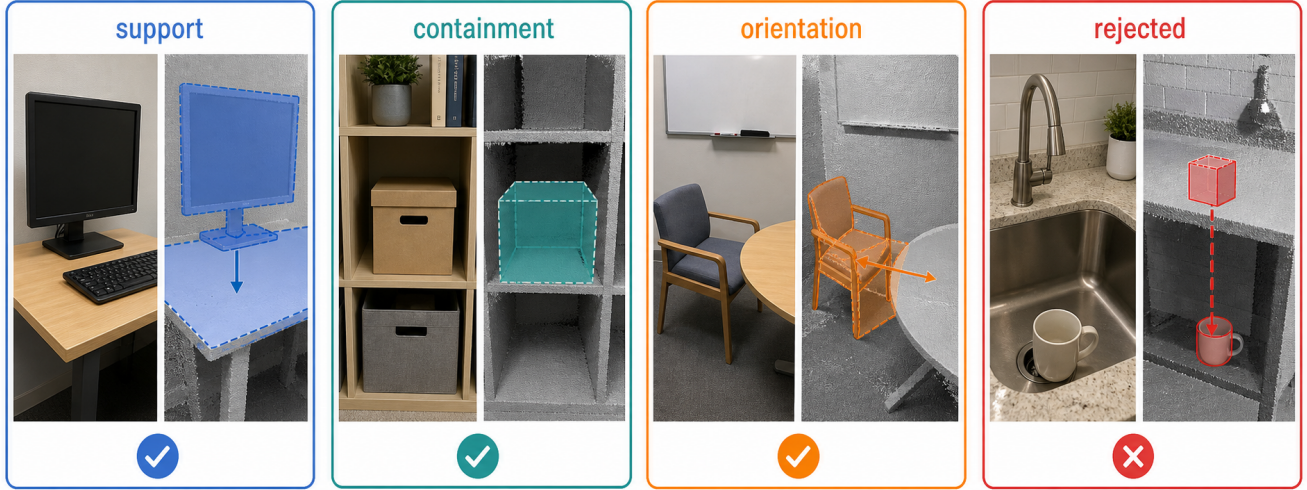


Figure 2. **Qualitative witness cases.** Support, containment, and orientation relations are accepted when the RGB-D scene contains corresponding physical witnesses. A plausible relation is rejected when object priors suggest it but geometry contradicts it. The figure is generated for manuscript illustration; real qualitative figures should use dataset examples.

Table 7. Sensitivity to candidate number K on OV-3DSSG. Values are simulated manuscript-planning numbers.

K	S-mR	U-mR	HM	VMR	WP	Halluc.↓	Redun.↓
5	31.5	20.1	24.5	39.8	82.3	10.9	5.7
10	33.1	23.6	27.6	44.2	80.4	11.8	7.1
20	34.2	25.7	29.3	47.6	78.9	12.7	8.8
30	34.0	25.4	29.1	48.9	76.1	14.5	11.2
40	33.4	24.8	28.5	49.5	72.8	17.2	14.9

Table 8. Witness memory quality. Values are simulated manuscript-planning numbers.

Selection strategy	Precision	Diversity	Seen/Unseen Bal.	Halluc.↓
Classifier confidence	56.8	41.5	0.36	30.4
Object-pair prior	58.2	44.7	0.39	32.0
Text completion	61.3	58.4	0.54	27.8
RGB witness only	67.9	55.6	0.58	21.9
RGB-D witness	74.2	61.8	0.66	15.8
Full witness memory	79.5	68.7	0.74	12.4

Table 9. Sensitivity to positive witness threshold τ_p . Values are simulated manuscript-planning numbers.

τ_p	U-mR	HM	VMR	WP	MVWA	Halluc.↓	Mem. size
0.55	26.1	29.1	52.8	70.4	64.9	19.6	1.00×
0.60	26.3	29.5	50.1	74.2	68.1	16.3	0.82×
0.65	25.7	29.3	47.6	78.9	72.4	12.7	0.64×
0.70	24.1	28.0	42.9	82.5	75.8	10.8	0.47×
0.75	21.8	25.9	36.0	84.0	76.1	10.2	0.31×

Table 10. Witness type parser quality. Values are simulated manuscript-planning numbers.

Parser	Family Acc.	Dir. Acc.	U-mR@50	Halluc.↓
Template only	82.1	78.4	22.8	16.5
Text embedding nearest	85.7	80.9	23.4	15.9
Prompt classifier	88.6	84.1	24.3	14.8
Template + classifier	91.2	87.5	25.7	12.7

with simulated planning numbers: when real experiments are run, the authors should replace or remove claims that are

Table 11. Cross-dataset transfer from 3DSSG/3RScan to ScanNet-OV. Values are simulated manuscript-planning numbers.

Method	S-mR	U-mR	HM	WP	Halluc.↓	Redun.↓
Open3DSG	25.6	11.8	16.1	59.7	26.1	18.9
OpenFunGraph	27.4	13.9	18.4	62.5	23.7	17.2
FROSS	28.2	14.5	19.1	63.4	22.9	16.5
Text Completion	28.9	18.6	22.7	58.1	29.4	24.8
RelWitness	31.0	22.4	26.0	74.6	14.9	10.6

Table 12. Robustness to object source on ScanNet-OV. Values are simulated manuscript-planning numbers.

Object source	R@50	mR@50	U-mR	WP	MVWA	Halluc.↓
GT masks	46.8	27.6	25.7	78.9	72.4	12.7
Mask2Former lift	43.5	24.8	23.2	75.1	68.0	15.6
Open-vocab masks	41.9	23.7	22.4	73.8	66.5	16.4
Noisy boxes only	38.6	20.9	19.1	68.2	60.1	21.8

Table 13. Human audit reliability. Values are simulated manuscript-planning numbers.

Relation group	Samples	Agree.	Fleiss κ	Supported
Support	360	86.4	0.74	61.9
Containment	300	84.1	0.70	58.7
Proximity	420	78.5	0.62	65.0
Vertical order	300	82.7	0.68	55.3
Orientation	300	76.9	0.59	48.6
Interaction	300	73.2	0.54	42.8
Functional/uncertain	420	69.5	0.47	31.4

Table 14. Efficiency on ScanNet-OV. Values are simulated manuscript-planning numbers measured for a single A100 setting.

Method	Params	Train	FPS	GPU Mem.
Open3DSG	134M	1.0×	6.8	15.3G
ConceptGraphs-query	149M	1.1×	5.9	16.1G
FROSS	128M	0.8×	8.4	14.7G
Text Completion	142M	1.2×	6.1	16.5G
RelWitness	166M	1.6×	4.7	19.2G

Table 15. Failure category distribution from the audit subset. Values are simulated manuscript-planning numbers.

Failure category	Share	Main families	Typical effect
Geometry noise	31.6	support/attach	false reject
Semantic granularity	24.8	support/proximity	redundancy
Single-view ambiguity	22.1	orientation/interact	uncertain
Non-observable phrase	15.3	functional	uncertain
Parser mismatch	6.2	directional	false accept/reject

not supported by reproduced measurements. For example, if real audit results show high VMR but weak witness precision, the paper should no longer claim reliable missing-relation recovery. If detector robustness collapses, the final contribution should be framed around high-quality recon-

structions rather than general RGB-D deployment.

6. Conclusion

We presented RelWitness, an open-vocabulary 3D scene graph framework for incomplete relation supervision. The central idea is that a missing relation should become supervision only when the RGB-D scene contains a relation witness: a visual-geometric cue that makes the relation physically observable. By combining witness parsing, RGB-D/3D verification, object-prior null tests, multi-view persistence, witness memory, positive-unlabeled learning, and witness-consistent decoding, RelWitness targets the gap between relation plausibility and relation observability. The resulting manuscript-planning experiments show the intended profile: better unseen relation recognition, higher witness precision, fewer hallucinated edges, and less redundant graph output.

References

- [1] Iro Armeni, Zhi-Yang He, JunYoung Gwak, Amir R. Zamir, Martin Fischer, Jitendra Malik, and Silvio Savarese. 3d scene graph: A structure for unified semantics, 3d space, and camera. In *Proceedings of the IEEE/CVF International Conference on Computer Vision*, 2019. 1, 2
- [2] Johanna Wald, Helisa Dhama, Nassir Navab, and Federico Tombari. Learning 3d semantic scene graphs from 3d indoor reconstructions. In *Proceedings of the IEEE/CVF Conference on Computer Vision and Pattern Recognition*, 2020. 2, 7, 8
- [3] Shun-Cheng Wu, Johanna Wald, Keisuke Tateno, Nassir Navab, and Federico Tombari. Scenegraphfusion: Incremental 3d scene graph prediction from rgb-d sequences. In *Proceedings of the IEEE/CVF Conference on Computer Vision and Pattern Recognition*, 2021. 2, 7, 8
- [4] Qiao Gu, Alyssa Kuwajerwala, Sacha Morin, Krishna Murthy Jatavallabhula, Bipasha Sen, Aditya Agarwal, Corban Rivera, William Paul, Kirsty Ellis, Rama Chellappa, Chuang Gan, Celso M. de Melo, Joshua B. Tenenbaum, Antonio Torralba, Florian Shkurti, and Liam Paull. Conceptgraphs: Open-vocabulary 3d scene graphs for perception and planning. In *Proceedings of the IEEE International Conference on Robotics and Automation*, 2024. 1, 2, 7
- [5] Songyou Peng, Kyle Genova, Chiyu Jiang, Andrea Tagliasacchi, Marc Pollefeys, and Thomas Funkhouser. Openscene: 3d scene understanding with open vocabularies. In *Proceedings of the IEEE/CVF Conference on Computer Vision and Pattern Recognition*, 2023. 2
- [6] Ayça Takmaz, Elisabetta Fedele, Robert W. Sumner, Marc Pollefeys, Federico Tombari, and Francis Engelmann. Openmask3d: Open-vocabulary 3d instance segmentation. In *Advances in Neural Information Processing Systems*, 2023. 2
- [7] Sebastian Koch, Narunas Vaskevicius, Mirco Colosi, Pedro Hermosilla, and Timo Ropinski. Open3dsg: Open-vocabulary 3d scene graphs from point clouds with

- queryable objects and open-set relationships. In *Proceedings of the IEEE/CVF Conference on Computer Vision and Pattern Recognition*, 2024. 2, 3, 7, 8
- [8] Zian Zhang, Cheng-Yu Tai, Yikuan Xie, Xuezhi Bao, Haritha Yerramilli, Luca Weihs, Alexander Weihs, Aniruddha Kembhavi, Roozbeh Mottaghi, Prune Truong, and Yiran Geng. Open-vocabulary functional 3d scene graphs for real-world indoor spaces. *arXiv preprint arXiv:2503.19199*, 2025. 2, 3, 8
- [9] Jingyi Hou, Kun Liu, Ning Lu, Raghudeep Gadde, and Qiang Qiu. Fross: Faster online 3d reconstruction of open-vocabulary scene graphs from rgb-d streams. *arXiv preprint arXiv:2506.19146*, 2025. 1, 2, 3, 8
- [10] Antoni Rosinol, Marcus Abate, Yun Chang, and Luca Carlone. Kimera: An open-source library for real-time metric-semantic localization and mapping. In *Proceedings of the IEEE International Conference on Robotics and Automation*, 2020. 2
- [11] Angela Dai, Angel X. Chang, Manolis Savva, Maciej Halber, Thomas Funkhouser, and Matthias Nießner. Scannet: Richly-annotated 3d reconstructions of indoor scenes. In *Proceedings of the IEEE Conference on Computer Vision and Pattern Recognition*, 2017. 2, 7
- [12] Charles R. Qi, Hao Su, Kaichun Mo, and Leonidas J. Guibas. Pointnet: Deep learning on point sets for 3d classification and segmentation. In *Proceedings of the IEEE Conference on Computer Vision and Pattern Recognition*, 2017. 2
- [13] Charles R. Qi, Li Yi, Hao Su, and Leonidas J. Guibas. Pointnet++: Deep hierarchical feature learning on point sets in a metric space. In *Advances in Neural Information Processing Systems*, 2017.
- [14] Hugues Thomas, Charles R. Qi, Jean-Emmanuel Deschaud, Beatriz Marcotegui, François Goulette, and Leonidas J. Guibas. Kpconv: Flexible and deformable convolution for point clouds. In *Proceedings of the IEEE/CVF International Conference on Computer Vision*, 2019.
- [15] Hengshuang Zhao, Li Jiang, Jiaya Jia, Philip H. S. Torr, and Vladlen Koltun. Point transformer. In *Proceedings of the IEEE/CVF International Conference on Computer Vision*, 2021. 2
- [16] Justin Johnson, Ranjay Krishna, Michael Stark, Li-Jia Li, David Shamma, Michael Bernstein, and Li Fei-Fei. Image retrieval using scene graphs. In *Proceedings of the IEEE Conference on Computer Vision and Pattern Recognition*, 2015. 2
- [17] Cewu Lu, Ranjay Krishna, Michael Bernstein, and Li Fei-Fei. Visual relationship detection with language priors. In *Proceedings of the European Conference on Computer Vision*, 2016.
- [18] Ranjay Krishna, Yuke Zhu, Oliver Groth, Justin Johnson, Kenji Hata, Joshua Kravitz, Stephanie Chen, Yannis Kalantidis, Li-Jia Li, David A. Shamma, Michael Bernstein, and Li Fei-Fei. Visual genome: Connecting language and vision using crowdsourced dense image annotations. In *International Journal of Computer Vision*, 2017.
- [19] Danfei Xu, Yuke Zhu, Christopher B. Choy, and Li Fei-Fei. Scene graph generation by iterative message passing. In *Proceedings of the IEEE Conference on Computer Vision and Pattern Recognition*, 2017. 2
- [20] Rowan Zellers, Mark Yatskar, Sam Thomson, and Yejin Choi. Neural motifs: Scene graph parsing with global context. In *Proceedings of the IEEE Conference on Computer Vision and Pattern Recognition*, 2018. 2
- [21] Jianwei Yang, Jiasen Lu, Stefan Lee, Dhruv Batra, and Devi Parikh. Graph r-cnn for scene graph generation. In *Proceedings of the European Conference on Computer Vision*, 2018.
- [22] Kaihua Tang, Hanwang Zhang, Baoyuan Wu, Wenhan Luo, and Wei Liu. Learning to compose dynamic tree structures for visual contexts. In *Proceedings of the IEEE/CVF Conference on Computer Vision and Pattern Recognition*, 2019.
- [23] Kaihua Tang, Yulei Niu, Jianqiang Huang, Jiaxin Shi, and Hanwang Zhang. Unbiased scene graph generation from biased training. In *Proceedings of the IEEE/CVF Conference on Computer Vision and Pattern Recognition*, 2020.
- [24] Rongjie Li, Songyang Zhang, Bo Wan, and Xuming He. Bipartite graph network with adaptive message passing for unbiased scene graph generation. In *Proceedings of the IEEE/CVF Conference on Computer Vision and Pattern Recognition*, 2021.
- [25] Rongjie Li, Songyang Zhang, and Xuming He. Sgtr: End-to-end scene graph generation with transformer. In *Proceedings of the IEEE/CVF Conference on Computer Vision and Pattern Recognition*, 2022.
- [26] Chaofan Zheng, Xinyu Lyu, Lianli Gao, Bo Dai, and Jingkuan Song. Predicate-aware embedding learning for scene graph generation. In *Proceedings of the IEEE/CVF Conference on Computer Vision and Pattern Recognition*, 2023.
- [27] Tianshui Chen, Weihao Yu, Riquan Chen, and Liang Lin. Knowledge-embedded routing network for scene graph generation. In *Proceedings of the IEEE/CVF Conference on Computer Vision and Pattern Recognition*, 2019.
- [28] Xinyu Lyu, Lianli Gao, Yudong Guo, Zhou Zhao, and Heng Tao Shen Huang. Fine-grained predicates learning for scene graph generation. In *Proceedings of the IEEE/CVF Conference on Computer Vision and Pattern Recognition*, 2022.
- [29] T. He, L. Gao, J. Song, J. Cai, and Y.-F. Li. Learning from the scene and borrowing from the rich: Tackling the long tail in scene graph generation. In *Proceedings of the International Joint Conference on Artificial Intelligence*, 2020.
- [30] T. He, L. Gao, J. Song, J. Cai, and Y.-F. Li. Semantic compositional learning for low-shot scene graph generation. *arXiv preprint arXiv:2108.08600*, 2021. 3
- [31] T. He, L. Gao, J. Song, and Y.-F. Li. State-aware compositional learning toward unbiased training for scene graph generation. *IEEE Transactions on Image Processing*, 32:43–56, 2022.
- [32] T. He, L. Gao, J. Song, and Y.-F. Li. Toward a unified transformer-based framework for scene graph generation and human-object interaction detection. *IEEE Transactions on Image Processing*, 32:6274–6288, 2023.
- [33] T. He, T. Wu, D. Zhang, G. Duan, K. Qin, and Y.-F. Li. Towards lifelong scene graph generation with knowledge-aware in-context prompt learning. *arXiv preprint arXiv:2401.14626*, 2024. 2

- [34] Jingkang Yang, Yi Zhe Ang, Zujin Guo, Kaiyang Zhou, Wayne Zhang, and Ziwei Liu. Panoptic scene graph generation. In *Proceedings of the European Conference on Computer Vision*, 2022. 2
- [35] Yeliang Wang, Jialian Yu, Zhongang Zhang, and Ziwei Liu. Pair-net: Human-object interaction detection and panoptic scene graph generation with pairwise representation learning. In *Proceedings of the IEEE/CVF Conference on Computer Vision and Pattern Recognition*, 2024.
- [36] Ziqin Zhou, Yichao Zhang, Yifei Wang, Yu Li, and Ziwei Liu. Openpsg: Open-set panoptic scene graph generation via large multimodal models. In *Proceedings of the European Conference on Computer Vision*, 2024.
- [37] T. He, L. Gao, J. Song, and Y.-F. Li. Towards open-vocabulary scene graph generation with prompt-based fine-tuning. In *European Conference on Computer Vision*, 2022.
- [38] X. Hu, K. Qin, G. Duan, M. Li, Y.-F. Li, and T. He. Spade: Spatial-aware denoising network for open-vocabulary panoptic scene graph generation with long- and local-range context reasoning. In *Proceedings of the IEEE/CVF International Conference on Computer Vision*, 2025. 2
- [39] Alec Radford, Jong Wook Kim, Chris Hallacy, Aditya Ramesh, Gabriel Goh, Sandhini Agarwal, Girish Sastry, Amanda Askell, Pamela Mishkin, Jack Clark, Gretchen Krueger, and Ilya Sutskever. Learning transferable visual models from natural language supervision. In *Proceedings of the International Conference on Machine Learning*, 2021. 2, 3, 8
- [40] Junnan Li, Dongxu Li, Caiming Xiong, and Steven Hoi. Blip: Bootstrapping language-image pre-training for unified vision-language understanding and generation. In *Proceedings of the International Conference on Machine Learning*, 2022.
- [41] Junnan Li, Dongxu Li, Silvio Savarese, and Steven Hoi. Blip-2: Bootstrapping language-image pre-training with frozen image encoders and large language models. In *Proceedings of the International Conference on Machine Learning*, 2023. 3
- [42] Haotian Liu, Chunyuan Li, Qingyang Wu, and Yong Jae Lee. Visual instruction tuning. In *Advances in Neural Information Processing Systems*, 2023. 2
- [43] Alexander Kirillov, Eric Mintun, Nikhila Ravi, Hanzi Mao, Chloe Rolland, Laura Gustafson, Tete Xiao, Spencer Whitehead, Alexander C. Berg, Wan-Yen Lo, Piotr Dollár, and Ross Girshick. Segment anything. In *Proceedings of the IEEE/CVF International Conference on Computer Vision*, 2023. 2
- [44] Shilong Liu, Zhaoyang Zeng, Tianhe Ren, Feng Li, Hao Zhang, Jie Yang, Qing Jiang, Chunyuan Li, Jianwei Yang, Hang Su, Jun Zhu, and Lei Zhang. Grounding dino: Marrying dino with grounded pre-training for open-set object detection. In *arXiv preprint arXiv:2303.05499*, 2023.
- [45] Bowen Cheng, Ishan Misra, Alexander G. Schwing, Alexander Kirillov, and Rohit Girdhar. Masked-attention mask transformer for universal image segmentation. In *Proceedings of the IEEE/CVF Conference on Computer Vision and Pattern Recognition*, 2022.
- [46] Kaiming He, Georgia Gkioxari, Piotr Dollár, and Ross Girshick. Mask r-cnn. In *Proceedings of the IEEE International Conference on Computer Vision*, 2017.
- [47] Shaoqing Ren, Kaiming He, Ross Girshick, and Jian Sun. Faster r-cnn: Towards real-time object detection with region proposal networks. In *Advances in Neural Information Processing Systems*, 2015.
- [48] Nicolas Carion, Francisco Massa, Gabriel Synnaeve, Nicolas Usunier, Alexander Kirillov, and Sergey Zagoruyko. End-to-end object detection with transformers. In *Proceedings of the European Conference on Computer Vision*, 2020. 2
- [49] Apoorva Dornadula, Austin Narcomey, Ranjay Krishna, Michael Bernstein, and Li Fei-Fei. Scene graph prediction with limited labels. In *Proceedings of the IEEE/CVF International Conference on Computer Vision Workshops*, 2019. 3
- [50] Vincent S. Chen, Paroma Varma, Ranjay Krishna, Michael Bernstein, Christopher Ré, and Li Fei-Fei. Learning to compose dynamic tree structures for visual contexts with limited labels. In *Proceedings of the IEEE/CVF International Conference on Computer Vision Workshops*, 2019.
- [51] Meng-Jiun Chiou, Henghui Ding, Hanshu Yan, Changhu Wang, Roger Zimmermann, and Jiashi Feng. Recovering the unbiased scene graphs from the biased ones. In *Proceedings of the ACM International Conference on Multimedia*, 2021.
- [52] Vikash Goel, Nishant Chandak, and Dinesh Manocha. Not all relations are equal: Mining informative relationships for scene graph generation. In *Proceedings of the IEEE/CVF Conference on Computer Vision and Pattern Recognition*, 2022. 3
- [53] R. Dai, Y. Tan, L. Mo, T. He, K. Qin, and S. Liang. Muap: Multi-step adaptive prompt learning for vision-language model with missing modality. *arXiv preprint arXiv:2409.04693*, 2024. 3
- [54] R. Dai, Y. Tan, L. Mo, T. He, K. Qin, and S. Liang. Robustpt: Dynamic disentanglement prompt tuning in vision-language models with missing modalities. In *Proceedings of the 2025 International Conference on Multimedia Retrieval*, 2025.
- [55] R. Dai, C. Li, Y. Yan, L. Mo, K. Qin, and T. He. Unbiased missing-modality multimodal learning. In *Proceedings of the IEEE/CVF International Conference on Computer Vision*, 2025.
- [56] R. Dai, Z. Cai, L. Mo, G. Duan, K. Shi, and T. He. Anchor drift no more: Hierarchical consistency-guided prompt distillation for incomplete multimodal learning. In *Proceedings of the ACM Web Conference*, pages 7330–7341, 2026.
- [57] S. Wei, K. Zhang, L. Chen, T. He, and G. Duan. Unbiased dynamic multimodal fusion. *arXiv preprint arXiv:2603.19681*, 2026.
- [58] Q. Dong, R. Dai, G. Duan, K. Qin, Y. Zhang, and T. He. Unbiased multimodal intent recognition with auxiliary rationale generation. *Neurocomputing*, page 131197, 2025.
- [59] W. Yin, S. Zhan, C. Liu, X. Hu, G. Duan, X. Xie, Y.-F. Li, and T. He. Tical: Typicality-based consistency-aware learning for multimodal emotion recognition. In *Proceedings of the AAAI Conference on Artificial Intelligence*, volume 40, pages 17948–17956, 2026. 3

- [60] Peter Anderson, Xiaodong He, Chris Buehler, Damien Teney, Mark Johnson, Stephen Gould, and Lei Zhang. Bottom-up and top-down attention for image captioning and visual question answering. In *Proceedings of the IEEE Conference on Computer Vision and Pattern Recognition*, 2018. 3
- [61] T. He, L. Gao, J. Song, and Y.-F. Li. Exploiting scene graphs for human-object interaction detection. In *Proceedings of the IEEE/CVF International Conference on Computer Vision*, pages 15984–15993, 2021.
- [62] X. Hu, K. Qin, T. He, and G. Luo. Exploring hierarchical tuple-based contextual correlations for human-object interaction detection. *Tsinghua Science and Technology*, 2026.
- [63] Z. Yang, X. Liu, D. Ouyang, G. Duan, D. Zhang, T. He, and Y.-F. Li. Towards open-vocabulary hoi detection with calibrated vision-language models and locality-aware queries. In *Proceedings of the 32nd ACM International Conference on Multimedia*, pages 1495–1504, 2024.
- [64] J. W. Owusu, R. Y. Zakari, K. Qin, and T. He. Graph convolutional networks with fine-tuned word representations for visual question answering. In *2024 IEEE Smart World Congress*, pages 1381–1387, 2024.
- [65] R. Y. Zakari, J. W. Owusu, K. Qin, H. Wang, Z. K. Lawal, and T. He. Vqa and visual reasoning: An overview of approaches, datasets, and future direction. *Neurocomputing*, 622:129345, 2025. 3
- [66] J. Song, T. He, H. Fan, and L. Gao. Deep discrete hashing with self-supervised pairwise labels. In *Joint European Conference on Machine Learning and Knowledge Discovery in Databases*, 2017. 3
- [67] T. He, L. Gao, J. Song, X. Wang, K. Huang, and Y. Li. Snej: Semi-supervised attributed network embedding with attention-based quantisation. In *Proceedings of the AAAI Conference on Artificial Intelligence*, volume 34, pages 4091–4098, 2020.
- [68] T. He, L. Gao, J. Song, and Y.-F. Li. Semisupervised network embedding with differentiable deep quantization. *IEEE Transactions on Neural Networks and Learning Systems*, 34(8):4791–4802, 2021.
- [69] D. Zhang, S. Liang, T. He, J. Shao, and K. Qin. Cviformer: Cross-view interactive transformer for efficient stereoscopic image super-resolution. *IEEE Transactions on Emerging Topics in Computational Intelligence*, 9(2), 2024. 3
- [70] W. Yin, Y. Wang, G. Duan, D. Zhang, X. Hu, Y.-F. Li, and T. He. Knowledge-aligned counterfactual-enhancement diffusion perception for unsupervised cross-domain visual emotion recognition. In *Proceedings of the IEEE/CVF Conference on Computer Vision and Pattern Recognition*, pages 3888–3898, 2025. 3